Title

Structural basis of gRNA stabilization and mRNA recognition in trypanosomal RNA editing

Journal

Science, 381(6653)

ISSN

0036-8075

Authors

Liu, Shiheng

Wang, Hong

Li, Xiaorun

et al.

Publication Date

2023-07-07

DOI

10.1126/science.adg4725

Peer reviewed

HHS Public Access

Author manuscript

Science. Author manuscript; available in PMC 2023 December 08.

Published in final edited form as:

Science. 2023 July 07; 381(6653): eadg4725. doi:10.1126/science.adg4725.

Structural basis of gRNA stabilization and mRNA recognition in trypanosomal RNA editing

Shiheng Liu[1,2,†], **Hong Wang**[3,†], **Xiaorun Li**[1,2], **Fan Zhang**[4], **Jane K.J. Lee**[1,2], **Zihang Li**[1,2], **Clinton Yu**[5], **Jason J. Hu**[1,2], **Xiaojing Zhao**[4], **Takuma Suematsu**[3], **Ana L. Alvarez-Cabrera**[1,2], **Qiushi Liu**[3], **Liye Zhang**[4,6], **Lan Huang**[5], **Inna Aphasizheva**[3], **Ruslan Aphasizhev**[3,7,*], **Z. Hong Zhou**[1,2,*]

[1]Department of Microbiology, Immunology, and Molecular Genetics, University of California, Los Angeles, CA, USA.

[2]California NanoSystems Institute, University of California, Los Angeles, CA, USA.

[3]Department of Molecular and Cell Biology, Boston University Medical Campus, Boston, MA, USA.

[4]School of Life Science and Technology, ShanghaiTech University, Shanghai, China.

[5]Department of Physiology and Biophysics, University of California, Irvine, CA, USA.

[6]Shanghai Clinical Research and Trial Center, Shanghai 201210, China.

[7]Department of Biochemistry, Boston University Medical Campus, Boston, MA, USA.

Abstract

INTRODUCTION: Discovered in the mitochondrion of *Trypanosoma brucei*, a protozoan parasite that causes African sleeping sickness, RNA editing denotes a spectrum of phylogenetically widespread and often mechanistically unrelated molecular processes that change RNA sequence. In trypanosomal RNA editing, gRNAs direct massive recoding of cryptic mitochondrial transcripts to generate mRNAs. Assembled into the partially defined editosome, two principal ribonucleoprotein particles execute an unconventional method of genetic information transfer from gRNA to mRNA. TheRNA-editing substrate-binding complex (RESC) stabilizes gRNAs and engages mRNAs. The RNA-editing catalytic complex (RECC) fulfills gRNA-programmed mRNA cleavage, uridine insertion or deletion, and relegation reactions.

[*]Corresponding author. ruslana@bu.edu (R.A.); hong.zhou@ucla.edu (Z.H.Z.).
[†]These authors contributed equally to this work.

Author contributions: Project initiation and supervision: Z.H.Z. and R.A.; Transgenic cell lines generation: H.W. and Q.L.; Biochemical analyses: H.W., I.A., and T.S.; Mass spectrometry: C.Y. and L.H.; Cryo-EM sample preparation: H.W.; EM sample evaluation and optimization: A.L.C., X.L., and S.L.; Cryo-EM imaging for RNase-treated samples: A.L.C. and X.L.; Data processing for RNase-treated samples: S.L., X.L. and A.L.C.; Cryo-EM imaging and data processing for mock-treated samples: S.L.; CryoID: X.L. and Z.L.; Protein atomic modeling: Z.L., J.K.J.L., H.W., J.J.H., and S.L.; Nucleotide identification and modeling: S.L.; eCLAP data generation: I.A.; eCLAP data analysis: F.Z., X.Z., and L.Z.; Data interpretation: S.L., Z.H.Z., R.A., I.A., J.J.H., J.K.J.L., and L.Z.; Figure preparation: S.L., J.K.J.L., J.J.H., I.A., F.Z., X.Z., L.Z., R.A., and Z.H.Z.; Movie preparation: J.J.H. and J.K.J.L.; Manuscript writing: S.L., L.Z., I.A., Z.H.Z., and R.A.

Competing interests: The authors declare no competing interests.

RATIONALE: Mitochondrial gRNA forms an imperfect duplex with mRNA precursor in which secondary structure defines multiple editing sites. To reveal gRNA stabilization and mRNA recognition mechanisms, we have determined atomic structures of three states of the RESC using cryogenic electron microscopy and characterized individual subunits' RNA-binding specificity.

RESULTS: Biochemical studies defined the RESC as a heterogenous assembly of ~18 proteins that enclose gRNAs and mRNAs. Prior work also demonstrated that the RESC1/2 dimer stabilizes gRNAs and most other proteins bind mRNAs. The structure of the six-member RESC-A shows how RESC2 RNA triphosphatase pseudoenzyme engulfs the triphosphorylated gRNA's 5′ end, and how the RESC5/6 dimer fastens the 3′ end. These contacts promote gRNA folding into a "hairpin-like" conformation and shield both termini from nucleases. The 10-polypeptide RESC-B structure suggests that a remodeling event recovers gRNA from the RESC-A "storage" mode and transitions the single-stranded molecule into mRNA proximity. In the process, the gRNA's 5′ end is ejected from the RESC2 triphosphate binding tunnel but the 3′ end remains wedged between RESC5 and RESC6, which are the only proteins shared between RESC-A and RESC-B. All RESC-B subunits, including RESC5/6, contact mRNA along a ~20-nucleotide segment. However, gRNA and mRNA do not interact within RESC-B boundaries.

A typical gRNA starts with an "anchor" fully complementary to the mRNA target; the adjacent "guiding" part pairs with mRNA sparsely and creates editing sites typified by single-stranded bulges and loops. A few nucleotides separate this "information-rich" sequence from the terminal uridine tail. Mechanistically, sequestering gRNA's "information-poor" 3′ end inside RESC-B allows guiding and anchor parts to hybridize with mRNA beyond RESC-B's surface. Apparently, RESC-B proteins recruit gRNAs and mRNAs irrespective of their sequences and position the two strands in a roughly antiparallel orientation, but distant enough to prevent spurious annealing within the complex. The exposed gRNA and mRNA regions likely sample each other until productive hybridization creates a substrate for the catalytic RECC complex.

CONCLUSION: The architectures of distinct RESC states reveal a diversity of protein folds that have been co-opted into the RNA editing machinery. We have discovered how common gRNA elements function in stabilizing this short molecule and engaging mRNA. Our results show that gRNA-mRNA recognition emanates from ribonucleoprotein complex remodeling rather than initiating base pairing of the anchor sequence with the mRNA target. Last, structural information on essential functional features, such as the RESC2 triphosphate binding site, may facilitate development of new trypanocides.■

Abstract

In *Trypanosoma brucei*, the editosome, composed of RNA-editing substrate-binding complex (RESC) and RNA-editing catalytic complex (RECC), orchestrates guide RNA (gRNA)–programmed editing to recode cryptic mitochondrial transcripts into messenger RNAs (mRNAs). The mechanism of information transfer from gRNA to mRNA is unclear owing to a lack of high-resolution structures for these complexes. With cryo–electron microscopy and functional studies, we have captured gRNA-stabilizing RESC-A and gRNA-mRNA–binding RESC-B and RESC-C particles. RESC-A sequesters gRNA termini, thus promoting hairpin formation and blocking mRNA access. The conversion of RESC-A into RESC-B or -C unfolds gRNA and allows mRNA selection. The ensuing gRNA-mRNA duplex protrudes from RESC-B, likely exposing editing sites to RECC-catalyzed cleavage, uridine insertion or deletion, and ligation. Our work reveals

a remodeling event facilitating gRNA-mRNA hybridization and assembly of a macromolecular substrate for the editosome's catalytic modality.

Graphical Abstract

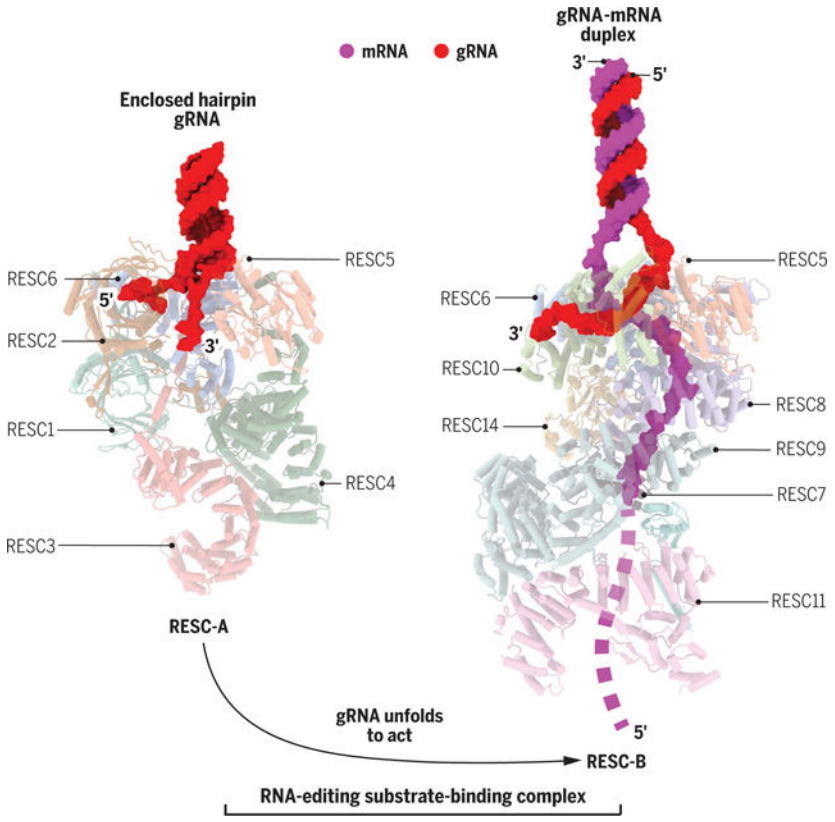

Structures of RESCs. (Left) RESC-A sequesters gRNA termini, promoting hairpin formation and blocking mRNA access. (Right) RESC-A conversion into RESC-B unfolds gRNA and allows mRNA recognition, likely exposing editing sites to RECC-embedded enzymes.

Kinetoplastids are a group of flagellated protozoans that infect humans and livestock in some of the most impoverished regions of the world. *Trypanosoma brucei* spp. cause African human and animal trypanosomiasis, a substantial health threat and economic burden, respectively, in sub-Saharan Africa. The toxicity and complex regimens of existing treatments call for identification of potential parasite-specific drug targets, among which the distinct organellar RNA-editing complexes stand prominent. In trypanosomes, RNA editing restores the protein coding capacity of mitochondrial cryptogenes by massive posttranscriptional insertions and deletions of uridines (uridine, U) (1, 2). Short noncoding RNAs bind to and program sequence changes in the mRNA. Astutely termed guide RNAs (gRNAs) are ~50–nucleotide (nt) molecules that feature a triphosphorylated 5′ end, followed by the "anchor" region complementary to mRNA target, the "guiding" part, and often an uridylated 3′ end (3–5). In massively edited (pan-edited) mRNAs, overlapping gRNAs sequentially bind to mRNA as recoding progresses from the 3′ to the 5′ end (6).

Discoveries of RNA editing and gRNAs in trypanosomes have laid the foundation for developing modern RNA-directed genome-and transcriptome-altering technologies.

The partially defined *T. brucei* editosome includes RNA-editing substrate-binding complex (RESC) and RNA-editing catalytic complex (RECC) (7–9). Molecular studies have implicated homologous binding partners RESC1 and RESC2, previously named GRBC1/2 (10) or GAP2/1 (11), in gRNA stabilization and demonstrated their presence in heterogeneous (0.3 to 1.2 MDa) ribonucleoproteins (RNPs) involving up to 18 polypeptides [RESC protein nomenclature is available in (8)] (10–12). The RNPs that contain the RESC1/2 dimer incorporate editing substrates (gRNAs and pre-edited mRNAs) and products (partially and fully edited mRNAs) (7, 12–14). Conversely, the RECC complex encloses enzymes performing gRNA-programmed mRNA cleavage, U insertions or deletions, and religation (15–17).

Efforts to understand editing mechanisms at the structural level remain limited to crystallographic studies of recombinantly produced individual enzymes (18–20) and factors (21–23). Previous electron microscopy (EM) attempts yielded negative-stain structures of the catalytic editing complex at ~30-Å resolution (24, 25). In this study, we combined biochemical, mass spectrometry, in vivo RNA profiling, and cryoID (26) approaches to capture three states of the RESC and reveal their atomic details by single-particle cryo–electron microscopy (cryo-EM).

Results

Capturing three states of RESC: RESC-A, RESC-B, and RESC-C

To produce isolates amenable to cryo-EM reconstitutions at near-atomic resolution, we initially Initially purified endogenous RESC2 (Fig. 1A and fig. S1) and separated the associated complexes by glycerol gradient and native polyacrylamide gel electrophoresis (PAGE) to resolve the predominant ~280 kDa and less abundant ~0.5 to 1.2 MDa complexes (Fig. 1B). Although the RESC1/2 dimer binds gRNAs in vitro (10, 27), distribution along the gradient shows that the most abundant ~280 kDa RESC1/2-containing particles are devoid of gRNAs, which are sequestered into complexes exceeding 400 kDa (Fig. 1B, bottom). To capture these larger gRNA-containing assemblies, we tested RESC2, RESC5, RESC9, and RESC14 isolates for RESC components and associated mRNA-processing complexes (fig. S2 and table S1). The RESC2-purified sample contained abundant RESC1/2 and KREH2 helicase, whereas both RESC9 and RESC14 isolates lacked RESC1 to RESC4 and RESC15 to RESC18, respectively. Compared with the others, the RESC5 complex comprised a more uniform set of RESC proteins and higher relative amount of the catalytic RECC (fig. S2). Size separation of RESC5 (Fig. 1C) demonstrated cosedimentation with RESC4 (Fig. 1D), which is predicted to interact with RESC1/2 and RESC5 (7, 13). Likewise, native PAGE revealed RESC5 presence in distinct complexes (Fig. 1D), of which RESC1/2 co-occupies the ~400-kDa particles and those exceeding 600 kDa (Fig. 1E). Informed by these findings, we selected RESC5 for cryo-EM analysis. To mitigate sample heterogeneity, mitochondrial lysate was treated with ribonucleases (RNases) before purification; this step reduced copurification of RESC12/12A mRNA-binding proteins

(28, 29) and mRNA editing (RECC and KREH2C) and processing (KPAC and PPsome) complexes (8) (Fig. 1F and table S2).

The RNase-treated RESC5 sample was evaluated by means of negative-stain EM and cryo-EM. The 2D averages of the cryo-EM particles revealed multiple species with miscellaneous shapes and dimensions (fig. S3, A and B). By combining these 2D classes for in-depth 3D analysis (fig. S4), we obtained a series of 3D structures, among which three were identified as RESC protein–containing complexes through the cryoID approach (26), and their atomic models were built. We designated them as RESC-A (3.7 Å), RESC-B (3.4 Å), and RESC-C (3.3 Å) (Fig. 1G, figs. S9 and S10, table S3, and movie S1). RESC-A contains RESC1 to RESC6, including the gRNA-stabilizing heterodimer RESC1/2. RESC-B incorporatesRESC5 to RESC11,RESC13, and RESC14, thus sharing the RESC5/6 heterodimer with RESC-A and possessing the mRNA-interacting RESC13 (28, 29). The smallest complex, RESC-C, consists of RESC5 to RESC8, RESC10, and RESC14; it may represent a RESC-B assembly intermediate or reflect RESC-B remodeling during editing (Fig. 1G and fig. S8). Most RESC components are composed of repetitive arrays of short amphiphilic α helices called HEAT repeats (also known as α solenoid) (fig. S11). HEAT repeats often form extended superhelical structures and mediate protein-protein interactions (30, 31), as observed here. Apparent molecular masses of RESC5 complexes agree with values calculated from structural models; RESC-A (~380 kDa) and RESC-B (~600 kDa) likely populate the upper band, with the lower band representing RESC-C (~270 kDa) (Fig. 1D and fig. S8).

Depletion of RESC12 and RESC12A from RESC5 isolates through RNase treatment (Fig. 1F) led us to inquire whether these paralogs that share 77% protein sequence identity and bind to pre-edited mRNA (28, 29) connect with RESC by means of an RNA component (Fig. 1F). For RESC12 and RES12A isolations without RNase treatment, paralog-specific peptide spectra counting showed reciprocal RESC12 and RESC12A relative abundances and their similar levels in RESC5 isolate (table S4). Overall, we conclude that RESC-A and RESC-B interact with KREH2 helicase and pre-edited mRNA binding factors, respectively, through RNA. As detailed below, the atomic models of RESC-A, RESC-B, and RESC-C reveal interactions among their subunits, the mechanisms of gRNA stabilization, and gRNA-mRNA recognition. Our analyses also suggest the mechanism by which a ribonucleoprotein substrate for the catalytic RECC assembles.

Structure of RESC-A

RESC-A contains six proteins and has dimensions of 180 by 115 by 95 Å (Figs. 1G and 2A). The presence of the RNA triphosphate tunnel metalloenzyme (TTM) domain (32) typifies RESC1 and RESC2; the latter also has an N-terminal armadillo (ARM) domain. RESC5 and RESC6 consist of β-propeller and superhelical HEAT domains, respectively. RESC3 and RESC4 are characterized by superhelical HEAT domains flanked by an N-terminal anchor and a C-terminal clip domain, respectively (fig. S11). RESC1 and RESC2 share a protein sequence identity of 31% and form a heterodimer (Fig. 2B and fig. S13B). A hairpin loop (amino acids 181 to 212) protruding from RESC2's TTM runs along the crevice outside the triphosphate tunnel of RESC1, yielding extensive hydrophobic interactions and

main chain–main chain hydrogen bonds (Fig. 2B, middle and right). Hydrogen bonds between RESC2's ARM and RESC1's TTM further enhance association (Fig. 2B, top left). Extensive RESC1/2 contacts likely underlie their interdependent persistence in the cell (11). The RESC1/2 heterodimer occupies the superhelical inner surface of RESC6's HEAT by means of the extended loop of RESC2's ARM, forming hydrogen bonds (Fig. 2C). RESC5 associates with RESC6 through hydrogen bonds and hydrophobic contacts (Fig. 2D), generating a positively charged crevice between RESC5 and RESC6 that is potentially receptive to RNA binding (Fig. 2E). RESC3 and RESC4 stabilize the orientations of RESC1/2 and RESC5/6 heterodimers (Fig. 2A and fig. S12, A and B).

Guide RNA interactions in RESC-A

The RESC-A structure described above was determined in the RNase-treated isolate (Figs. 1F and 2A, and figs. S4 and S5). Because molecular studies identified RESC1/2 as the key gRNA-stabilizing element (10), we next isolated RESC5 from mock-treated lysate and determined RESC-A structure with gRNA at 3.7-Å resolution (Fig. 3A, figs. S6 and S7, and movie S2). The overall structures are similar (Fig. 3B, left), except that disordered loops close to gRNA in RESC1 and RESC2 become organized and visible in the presence of gRNA (Fig. 3B, inset). The triphosphate binding tunnel of RESC2 engulfs the gRNA's 5′ end while the 3′ end docks into the crevice formed by RESC5 and RESC6 (Fig. 3, A and C). Specifically, the gRNA's 5′ triphosphate and conserved transcription initiation sequence contact the triphosphate binding tunnel, whereby the "anchor" and "guiding" regions hybridize into an ~18–base pair (bp) stem (Fig. 3D) reminiscent of gRNA folding in solution (33, 34). The locking of anchor and guiding regions into a hairpin suggests that gRNA must undergo a drastic conformational change to recognize mRNA. In addition to the 5 nt at the 3′ end lining up the crevice between RESC5/6, a total of 47 nt were modeled for gRNA in RESC-A (Fig. 3D). Accounting for the unstructured loop region, the RESC-bound gRNA matches the median 49-nt length of encoded gRNA sequences (35). Our findings imply that a hairpin conformation and 3′-end shielding by RESC5/6 render gRNA refractory to 3′-to-5′ degradation (4, 36, 37). We conclude that RESC-A, rather than solely the RESC1/2 heterodimer (10, 11, 27), is the gRNA-stabilizing particle.

gRNA is the only class of mitochondrial transcripts that retains 5′ triphosphate characteristic of transcription start site (3, 38), whereas the nonencoded 3′ U tail is added by the processome after precursor trimming (4, 5). To investigate the functional importance of the triphosphate binding by RESC2, we superimposed RESC1 and RESC2 TTM domains with Cet1 mRNA triphosphatase from *Saccharomyces cerevisiae* (32). Structural comparisons and sequence alignments of *T. brucei* and related parasite *Leishmania major* proteins show substitutions of two glutamic acids in the catalytic metal binding triad (E305-E307-E496; Cet1 numbering) that typify RESC1 and RESC2 as hydrolytically inactive pseudoenzymes (Fig. 3, E to G). The lack of phosphatase activities in RESC5 isolate and reconstituted RESC1/2 heterodimer support this conclusion (fig. S13). However, in the gRNA-occupied RESC2 TTM tunnel, positively charged residues (K311, R402, and R424; RESC2 numbering) form hydrogen bonds with the 5′ triphosphate moiety (Fig. 3, D and F). In RESC1, substitutions of potential triphosphate binding positions (R393 and K456; Cet1 numbering) by acidic or polar side chains (Fig. 3G) likely explain the lack of

gRNA occupancy (Fig. 3A). To test the essentiality of triphosphate contacts, we constructed cell lines for inducible overexpression of RESC2 mutants and tested their growth kinetics. Replacing E240A/N242A, residues in positions structurally homologous to Cet1 catalytic metal-binding side chains E305/E307, exerted no growth inhibition, which is consistent with the lack of a Mg^{2+}-binding site in RESC2 (Fig. 3, F and G). By comparison, mutations of triphosphate binding amino acids caused growth-inhibition phenotypes ranging from mild (K311A) to moderate (R402A/K406A) to severe (R424A) (Fig. 3H). As a control, R408A mutation in RESC1 (corresponding to R424A in RESC2) produced no discernible growth defect (fig. S14).

The long-debated U-tail function (3, 5, 39, 40) compelled a closer scrutiny of the 3′-end binding in the RESC5/6 crevice (Figs. 2E and 3, C and D). Ultraviolet (UV) irradiation of live parasites and sequencing of RNAs cross-linked to RESC1/2 and RESC5/6 (table S5) demonstrate that RESC-A shields the entire gRNA and indicate that RESC5 binds longer gRNA fragments than RESC2 (Fig. 3I). The difference emanates from RESC5-bound gRNAs possessing extended U tails (Fig. 3J). Consistent with uridylation patterns of predicted gRNAs versus gRNA-like molecules encoded by pseudo-gRNA genes (35), we found that RESC5 functionally selects gRNAs with longer U tails (Fig. 3K). Conversely, the lack of U-enriched motifs in RESC5-bound fragments stipulates a “molecular ruler” mechanism of gRNA selection: The length, rather than the sequence of nonencoded additions, delivers the 3′ end into the crevice between RESC5 and RESC6 (Fig. 3C). Taken together, our structural and functional data show that RESC-A selects gRNA by recognizing the 5′ triphosphate and accommodating a defined length and the capacity to fold into a hairpin-like conformation.

mRNA recognition in RESC-B

We also determined structures of RESC-B from RNase- and mock-treated RESC5 isolates. Although the latter has extended RNA densities and additional protein components, their overall structures are similar. The following description refers to their common features unless otherwise stated: RESC-B shares RESC5/6 heterodimer with RESC-A and contains additional components RESC7 to RESC14 [Figs. 1G (RNase-treated) and 4A (mock-treated) and movie S3]. Multiple helix-loop-helix structural motifs populate subunits RESC7–12 (fig. S11), with RESC8 to RESC12 forming extended superhelical HEAT domains. RESC13’s N-terminal RGG and C-terminal RRM motifs, both implicated in mRNA binding (41), are present in the structure of mock-treated RESC-B; only the RGG domain is visible in RNase-treated RESC-B. The RESC14 phytanoyl-CoA dioxygenase pseudoenzyme’s phyH domain is wedged between RESC6, RESC8, and RESC10 (Fig. 4A and fig. S12, C and D).

Two RNA strands are embedded in RESC-B. The shorter fragment contacts RESC5, RESC6, and RESC10 (Fig. 4, A and B, and fig. S12C), with nucleotides −16 to −12 (we designate position −1 as the 3′ end of visible RNA) being stacked between RESC5 and RESC6 (Fig. 4D), which mimics gRNA binding in RESC-A (Fig. 3, C and D). Therefore, this nucleotide strand was tentatively designated gRNA. In contrast to RESC-A, the 5′ gRNA nucleotides exiting fromRESC5/6 are not visible in RNase-treated RESC-B, whereas

the 3′ nucleotides extend further and interact with RESC10 (Fig. 4, A and D). Comparison of RESC-A and RESC-B suggests gRNA transition from a hairpin in RESC-A (Fig. 3, B to D) into single-stranded conformation in RESC-B (Fig. 4, A, B, and D). The enduring gRNA attachment to RESC5/6 during remodeling renders the stability of this interaction as a quality checkpoint for tunneling of properly 3′-processed molecules into the editing cascade.

RNA strand modeling and in vivo RNA-protein cross-linking data suggest that mRNA fragments account for the longer nucleotide segment traversing the entire RESC-B and interacting with all proteins (Fig. 4, A, C, E, H, and I, and fig. S12, D to F). The unmodeled 5′moiety runs through the interval between the RGG and RRM domain of RESC13 and further associates with the inner surface of RESC11's HEAT superhelix (Fig. 4, F and G). Heading toward the 3′ end, the mRNA is sequentially shielded by the superhelical inner surface of the HEAT repeats of RESC9, RESC8, and RESC6. This shielding is consistent with residual RNA moiety in the RNase-treated RESC-B (Fig. 1G, middle). In RESC-B, the mRNA's 3′ region is positioned in proximity (~30 Å) to the 5′ end of the single-stranded gRNA fragment unwound by RESC5, RESC6, and RESC10 (Fig. 4B). This mutual orientation potentially allows gRNA and mRNA to hybridize beyond the RESC-B surface.

gRNA-mRNA duplex scaffolding by RESC-B

Our cryo-EM structures show gRNA binding by RESC1/2 and RESC5/6 in RESC-A, and a continued gRNA engagement with RESC5/6 and additional interactions with RESC10 in RESC-B, all subunits of which also contact mRNA. However, sequence diversity of the endogenous transcripts impeded identification by cryo-EM of RNAs bound to each protein. To directly identify RNAs bound by individual RESC components, we carried out UV crosslinking of live parasites and purification of RNA-protein cross-links, RNA fragmentation, and sequencing (figs. S1 and S15A and table S5) (42). Consistent with our structures, RESC1 and RESC2 (RESC-A) display strong preference for gRNAs; RESC5, RESC6 (RESC-A and RESC-B), and RESC10 (RESC-B) cluster in the intermediate range commensurate with dual gRNA-mRNA binding modality; RESC-B–specific RESC7 to RESC14 predominantly cross-link to mRNAs (Fig. 4H). These data confirm the identity of the nucleotide strand held by RESC5/6/10 as gRNA (Fig. 4D) and the strand traversing the entire RESC-B as mRNA (Fig. 4A).

By forming an ~11-bp "anchor" duplex, which lengthens as U insertions and deletions extend complementarity with mRNA, gRNA initially recognizes cognate mRNA. Considering the lack of gRNA-mRNA pairing within RESC-B, we next assessed editing prevalence in mRNA fragments cross-linked to RESC-B proteins. The ratios of fully edited sequences to all reads derived from pan-edited mRNAs meeting coverage thresholds, uS12m (Fig. 4I), A6, and CO3, and from moderately edited CYB mRNA (fig. S15B and table S5), demonstrate that RESC12/12A paralogs and RESC13 display strongest preference for pre-edited mRNAs. The extent of editing increases in RESC14, whose suppression spares initiation but blocks editing progression (43, 44). As expected from our structures, edited sequences are most represented among RNAs cross-linked to gRNA-mRNA–binding

RESC5, RESC6, and RESC10 (Fig. 4I). Longitudinal mapping of RESC5 and RESC12 (Fig. 4J) and other RESC-B proteins (fig. S16) in vivo occupancies of uS12m mRNA further corroborates their aggregate binding preferences ranging from mostly pre-edited (RESC11/12/13) to partially edited (RESC5/6/10) sequences.

A gRNA-mRNA duplex protruding from the RESC5/6/10 cluster would be expected from structural and RNA profiling data. Local 3D classification of RESC-B particles indeed shows an extended gRNA-mRNA duplex (Fig. 5 and fig. S10J). The resultant reconstitutions traced a nearly complete 43-nt gRNA exiting from RESC-B and forming a 24-bp duplex with the 3′ part of the contiguous 51-nt mRNA fragment (Fig. 5A).

In typical gRNA, the guiding part is separated from the U tail by a few nucleotides that cannot pair with mRNA (35). Mechanistically, sequestering gRNA's "information-poor" 3′ end by RESC5/6/10 allows guiding and anchor parts to hybridize with mRNA beyond RESC-B surface, hence, accessible to RECC (Fig. 5C). It follows that RESC5/6/10 likely retains the U tail and adjacent nonguiding nucleotides as editing events take place between the 5′ anchor and gRNA's 3′ end. Because the mRNA is cleaved at each editing site, RESC-B contacts with single-stranded gRNA 3′ and mRNA 5′ regions likely tether mRNA cleavage fragments to gRNA. As documented by "precleaved" editing assays, such tethering stimulates U insertion, U deletion, and RNA ligation activities (45–47). Collectively, our findings introduce RESC-B as the probable substrate for the catalytic RECC complex. Upon completion of editing directed by a single gRNA, RESC-Bmay also expose the double-stranded region formed by gRNA and fully edited mRNA to postediting transactions.

Discussion

By using the cryoID approach, we have identified and built atomic models of three RNA-editing substrate-binding complexes—RESC-A, RESC-B, and RESC-C—from *T. brucei* mitochondrion. Information stored in minicircle and maxicircle genomes conflates during U insertion and deletion editing, whereby gRNAs produced from the former direct posttranscriptional recoding of cryptic transcripts encoded in the latter. The RESC molecular machines pairing hundreds of gRNAs with their targets are key to this broadly important process. In RESC-A composed of RESC1 to RESC6, RESC2 pseudotriphosphatase sequesters gRNA's 5′end into the triphosphate binding tunnel. Homologous binding partner RESC1 attaches RESC2 to RESC-A, wherein RESC5 and RESC6 affix gRNA's 3′ end by selecting molecules with longer U tails. The ensuing hairpin formation and protein contacts protect gRNA against 3′-to-5′ degradation in a plausibly inactive conformation where by the anchor hybridizes with the guiding region. Such "closed" conformation implies that gRNA remodeling precedes mRNA recognition. In RESC-B, composed of RESC5 to RESC14, we observed an mRNA fragment traversing the entire complex. An extensive hydrogen-bonding network fastens mRNA to every protein and positions its 3′ part close to a single-stranded gRNA segment unwound by interactions with RESC5, RESC6, and RESC10. Smaller RESC-C also contains gRNA and mRNA; whether this abundant particle represents a stable intermediate in the transition from RESC-A to RESC-B, or reflects RESC-B disassembly during postediting remodeling—e.g., pre-edited mRNA moving out of RESC12/12A—remains to be established.

Consistent with our atomic models, in vivo RNA-occupancy profiling discerned RESC components into preferential gRNA (RESC1/2), dual gRNA-mRNA(RESC5,RESC6, andRESC10), and pre-edited mRNA (RESC7 to RESC9 and RESC11 to RESC14) binding factors (Fig. 4H). We observed the least editing in mRNA fragments bound to RESC12 and RESC13, which are distal to gRNA in the RESC-B structure, and the most in those cross-linked to gRNA-proximal RESC5, RESC6, and RESC10 (Fig. 4I). The extent of U insertions and deletions gradually increases from the 5′ mRNA section sequestered by the RESC12/13 “entry” cluster toward the RESC5/6/10 “exit” module. Apparently, the RESC-B complex tethers gRNA’s 3′ end and pre-edited transcript to facilitate mRNA recognition by the anchor. The resultant imperfect mRNA-gRNA duplex protrudes from RESC-B surface (Fig. 5), exposing editing sites defined by a single gRNA to transiently binding and dissociating insertion- and deletion-specific RECC complexes (48, 49) and, possibly, to postediting transactions. For example, during pan-editing that involves multiple overlapping gRNAs, the initiating gRNA directs sequence changes that create a binding site for the next one (6). However, initiating gRNA must be dislodged from the edited mRNA before the next one anneals, and this may involve RESC-A and RESC-B cycling or RESC-B reduction into RESC-C. It is also plausible that translation initiation would require gRNA clearing from the initiation codon created by editing (50, 51).

Because RNA processing complexes typically undergo transient rearrangements implemented by molecular motors, the structures of stable particles suggest that RESC-A remodeling into RESC-B extracts gRNA’s 5′ end from the RESC2 triphosphate tunnel and ejects subunits RESC1–4 to unfold the gRNA hairpin. To transform RESC-A to RESC-B, the following displacements ought to occur on the basis of the structural comparison by shared components RESC5 and RESC6 (Fig. 6A, left): RESC10 and RESC14 will roughly occupy the position of RESC2 and RESC1, respectively (Fig. 6A, middle); RESC7 and RESC8 will replace RESC3 and RESC4 (Fig. 6A, right); and RESC2 displacement yields the superhelical inner surface of RESC6, which binds to mRNA’s 5′ segment in RESC-B (Fig. 6B).

Integration of biochemical data and structural analyses enables understanding of RESC assembly and rearrangements during the editing process (Fig. 6C). Separation of RESC2-associated complexes detects heterogeneous species with apparent molecular masses from ~280 kDa to ~1.2 MDa (Fig. 1) and demonstrates that the most abundant ~280 kDa particle lacks gRNAs. This correlates with the RESC-A cryo-EM structure, indicating that gRNA is sequestered into RESC-A during assembly from RESC1/2, RESC5/6, and RESC3 and RESC4 (Fig. 6C, left middle). Our results demonstrate a prominent RNA-dependent interaction between RESC-A and KREH2 RNA helicase, implicating this molecular motor in RESC-A assembly (Fig. 1, A to F). Conversely, undetectable KREH2 levels in RESC9 and RESC14 complexes suggest that the helicase dissociates from RESC-A during remodeling into RESC-B (table S1). In RESC-A, gRNA anchor and guiding regions fold into a hairpin, whereas the uridylated 3′ end is affixed in the crevice between RESC5 and RESC6 (Fig. 6C, left middle). A single-stranded 3′ end is required for recognition by KREH2, which is capable of unwinding double-stranded RNA (52, 53) and may unfold the hairpin to initiate RESC-A remodeling into RESC-B (Fig. 6C, right middle). In this scenario, recognition by KREH2 may select RESC5/6-bound gRNAs with longer U tails

(Fig. 3J) as a quality checkpoint of RESC-A assembly. Collectively, our findings highlight KREH2 helicase as the probable remodeler facilitating the transition from RESC-A to RESC-B. We postulate that RESC-B is the editing-competent substrate of the RECC catalytic complex, for which our structures reveal an unobstructed approach path to the gRNA-mRNA hybrid.

Materials and methods summary

Purification of the T. brucei RESC complex

For protein affinity purification and enhanced in vivo UV cross-linking/affinity purification/RNA sequencing (eCLAP), we introduced a CTS tag (combinatorial affinity tag consisting of 10 histidines, protein C peptide epitope, and TwinStrep peptide) (fig. S1A) at the C-termini of established RESC proteins (8). Protein-RNA adducts were purified by means of sequential streptavidin and metal affinity pulldowns and SDS-PAGE. RNA fragments were released through protease digestion and sequenced, as described in supplementary materials. Protein complexes were purified with tandem affinity chromatography from enriched mitochondrial fraction of procyclic (insect) form of *T. brucei* Lister 427 strain and analyzed as described in the supplementary materials.

EM grid preparation, imaging, data processing, and modeling

Cryo-EM grids of both RNase-treated and mock-treated samples were plunge-frozen into precooled, liquefied ethane using Vitrobot Mark IV, screened with FEI TF20, and imaged by using an FEI Titan Krios electron microscope. Data processing of the RNase-treated dataset yielded three final maps with average resolution (FSC 0.143) of 3.4, 3.7, and 3.3 Å, respectively. These maps were identified through the CryoID approach and modeled as RESC1–6–containing RESC-A (3.7 Å), RESC5–14–containing RESC-B (3.4 Å), and RESC5–8,10,14–containing RESC-C (3.3 Å). In combination with the mock-treated RESC-A/B/C, we were able to identify a “closed” gRNA in RESC-A and gRNA-mRNA duplex in RESC-B/C. Details of EM grid preparation, imaging, data processing, and modeling are described in the supplementary materials.

Data and materials availability:

The cryo-EM maps and atomic coordinates have been deposited to the EMDB (EMD-29308, EMD-29314, EMD-29305, EMD-29311, EMD-29316, EMD-29306 for RESC-A, -B, and -C with and without RNase treatment) and PDB (8FNC, 8FNI, 8FN4, 8FNF, 8FNK, 8FN6 for RESC-A, -B, and -C, with and without RNase treatment) databases, respectively, and will be released at time of publication. The raw FASTQ files produced by eCLAP experiments are deposited into the NCBI SRA database under accession number PRJNA879925. Scripts for data analysis and visualization are available at Zenodo (54). Mass spectrometry data have been deposited to the ProteomeXchange Consortium with the dataset identifier PXD039156.

Supplementary Material

Refer to Web version on PubMed Central for supplementary material.

ACKNOWLEDGMENTS

We thank Y. He and Y.-T. Liu for evaluating samples at the early stage of this project; W. Lan for initial atomic model–building efforts for part of RESC8, RESC9, and RESC14 in RESC-B structure obtained from RNase-treated isolate; A. Vacas for assistance with transgenic cell lines; and S. Shuman and J. C. Samuelson for discussions. We also thank the high-performance computing (HPC) platform of ShanghaiTech University for support.

Funding:

NIH grants R35GM145249 and R01GM074830 were given to L.H., RO1AI113157 to I.A., RO1AI101057 and R01AI152408 to R.A., and R01GM071940 to Z.H.Z. L.Z. is supported by National Natural Science Foundation of China (grant 31871332). We acknowledge the use of resources in the Electron Imaging Center for Nanomachines, supported by UCLA, and grants from NIH (S10RR23057, S10OD018111, and U24GM116792) and NSF (DBI-1338135 and DMR-1548924).

REFERENCES AND NOTES

1. Benne R. et al. , Major transcript of the frameshifted coxII gene from trypanosome mitochondria contains four nucleotides that are not encoded in the DNA. Cell 46, 819–826 (1986). doi: 10.1016/0092-8674(86)90063-2; [PubMed: 3019552]
2. Feagin JE, Abraham JM, Stuart K, Extensive editing of the cytochrome c oxidase III transcript in Trypanosoma brucei. Cell 53, 413–422 (1988). doi: 10.1016/0092-8674(88)90161-4; [PubMed: 2452697]
3. Blum B, Bakalara N, Simpson L, A model for RNA editing in kinetoplastid mitochondria: “guide” RNA molecules transcribed from maxicircle DNA provide the edited information. Cell 60, 189–198 (1990). doi: 10.1016/0092-8674(90)90735-W; [PubMed: 1688737]
4. Suematsu T. et al. , Antisense Transcripts Delimit Exonucleolytic Activity of the Mitochondrial 3′ Processome to Generate Guide RNAs. Mol. Cell 61, 364–378 (2016). doi: 10.1016/j.molcel.2016.01.004; [PubMed: 26833087]
5. Blum B, Simpson L, Guide RNAs in kinetoplastid mitochondria have a nonencoded 3′ oligo(U) tail involved in recognition of the preedited region. Cell 62, 391–397 (1990). doi: 10.1016/0092-8674(90)90375-O; [PubMed: 1695552]
6. Maslov DA, Simpson L, The polarity of editing within a multiple gRNA-mediated domain is due to formation of anchors for upstream gRNAs by downstream editing. Cell 70, 459–467 (1992). doi: 10.1016/0092-8674(92)90170-H; [PubMed: 1379519]
7. Aphasizheva I. et al. , RNA binding and core complexes constitute the U-insertion/deletion editosome. Mol. Cell. Biol. 34, 4329–4342 (2014). doi: 10.1128/MCB.01075-14; [PubMed: 25225332]
8. Aphasizheva I. et al. , Lexis and Grammar of Mitochondrial RNA Processing in Trypanosomes. Trends Parasitol. 36, 337–355 (2020). doi: 10.1016/j.pt.2020.01.006; [PubMed: 32191849]
9. McDermott SM, Luo J, Carnes J, Ranish JA, Stuart K, The Architecture of Trypanosoma brucei editosomes. Proc. Natl. Acad. Sci. U.S.A. 113, E6476–E6485 (2016). doi: 10.1073/pnas.1610177113; [PubMed: 27708162]
10. Weng J. et al. , Guide RNA-binding complex from mitochondria of trypanosomatids. Mol. Cell 32, 198–209 (2008). doi: 10.1016/j.molcel.2008.08.023; [PubMed: 18951088]
11. Hashimi H, Cicová Z, Novotná L, Wen YZ, Lukes J,Kinetoplastid guide RNA biogenesis is dependent on subunits of the mitochondrial RNA binding complex 1 and mitochondrial RNA polymerase. RNA 15, 588–599 (2009). doi:10.1261/rna.1411809; [PubMed: 19228586]
12. Panigrahi AK et al. , Mitochondrial complexes in Trypanosoma brucei: A novel complex and a unique oxidoreductase complex. Mol. Cell. Proteomics 7, 534–545 (2008). doi: 10.1074/mcp.M700430-MCP200; [PubMed: 18073385]
13. Ammerman ML et al. , Architecture of the trypanosome RNA editing accessory complex, MRB1. Nucleic Acids Res. 40, 5637–5650 (2012). doi: 10.1093/nar/gks211; [PubMed: 22396527]
14. Read LK, Lukeš J, Hashimi H, Trypanosome RNA editing: The complexity of getting U in and taking U out. Wiley Interdiscip. Rev. RNA 7, 33–51 (2016). doi: 10.1002/wrna.1313; [PubMed: 26522170]

15. Rusché LN, Cruz-Reyes J, Piller KJ, Sollner-Webb B,Purification of a functional enzymatic editing complex from Trypanosoma brucei mitochondria. EMBO J. 16, 4069–4081 (1997). doi: 10.1093/emboj/16.13.4069; [PubMed: 9233816]

16. Panigrahi AK et al. , Identification of novel components of Trypanosoma brucei editosomes. RNA 9, 484–492 (2003). doi: 10.1261/rna.2194603; [PubMed: 12649499]

17. Aphasizhev R. et al. , Isolation of a U-insertion/deletion editing complex from Leishmania tarentolae mitochondria. EMBO J. 22, 913–924 (2003). doi: 10.1093/emboj/cdg083; [PubMed: 12574127]

18. Deng J, Ernst NL, Turley S, Stuart KD, Hol WG,Structural basis for UTP specificity of RNA editing TUTases from Trypanosoma brucei. EMBO J. 24, 4007–4017 (2005). doi: 10.1038/sj.emboj.7600861; [PubMed: 16281058]

19. Deng J, Schnaufer A, Salavati R, Stuart KD, Hol WG,High resolution crystal structure of a key editosome enzyme from Trypanosoma brucei: RNA editing ligase 1. J. Mol. Biol. 343, 601–613 (2004). doi: 10.1016/j.jmb.2004.08.041; [PubMed: 15465048]

20. Stagno J, Aphasizheva I, Bruystens J, Luecke H,Aphasizhev R, Structure of the mitochondrial editosome-like complex associated TUTase 1 reveals divergent mechanisms of UTP selection and domain organization. J. Mol. Biol. 399, 464–475 (2010). doi: 10.1016/j.jmb.2010.04.021; [PubMed: 20403364]

21. Wu M. et al. , Structures of a key interaction protein from the Trypanosoma brucei editosome in complex with single domain antibodies. J. Struct. Biol. (2010).

22. Park YJ et al. , The structure of the C-terminal domain of the largest editosome interaction protein and its role in promoting RNA binding by RNA-editing ligase L2. Nucleic Acids Res. 40, 6966–6977 (2012). doi: 10.1093/nar/gks369; [PubMed: 22561373]

23. Shaw PL et al. , Structures of the T. brucei kRNA editing factor MRB1590 reveal unique RNA-binding pore motif contained within an ABC-ATPase fold. Nucleic Acids Res. 43, 7096–7109 (2015). doi: 10.1093/nar/gkv647; [PubMed: 26117548]

24. Golas MM et al. , Snapshots of the RNA editing machine in trypanosomes captured at different assembly stages in vivo. EMBO J. 28, 766–778 (2009). doi: 10.1038/emboj.2009.19; [PubMed: 19197238]

25. Li F. et al. , Structure of the core editing complex (L-complex) involved in uridine insertion/deletion RNA editing in trypanosomatid mitochondria. Proc. Natl. Acad. Sci. U.S.A. 106, 12306–12310 (2009). doi: 10.1073/pnas.0901754106; [PubMed: 19590014]

26. Ho CM et al. , Bottom-up structural proteomics: cryoEM of protein complexes enriched from the cellular milieu. Nat. Methods 17, 79–85 (2020). doi: 10.1038/s41592-019-0637-y; [PubMed: 31768063]

27. Dolce LG, Nesterenko Y, Walther L, Weis F, Kowalinski E,Structural basis for guide RNA selection by the RESC1-RESC2 complex. Nucleic Acids Res. 51, 4602–4612 (2023). doi: 10.1093/nar/gkad217; [PubMed: 36999600]

28. Dixit S. et al. , Differential Binding of Mitochondrial Transcripts by MRB8170 and MRB4160 Regulates Distinct Editing Fates of Mitochondrial mRNA in Trypanosomes. mBio 8, e02288–16 (2017). doi: 10.1128/mBio.02288-16; [PubMed: 28143982]

29. Kafková L. et al. , Functional characterization of two paralogs that are novel RNA binding proteins influencing mitochondrial transcripts of Trypanosoma brucei. RNA 18, 1846–1861 (2012). doi: 10.1261/rna.033852.112; [PubMed: 22898985]

30. Andrade MA, Petosa C, O'Donoghue SI, Müller CW, Bork P, Comparison of ARM and HEAT protein repeats. J. Mol. Biol. 309, 1–18 (2001). doi: 10.1006/jmbi.2001.4624; [PubMed: 11491282]

31. Neuwald AF, Hirano T, HEAT repeats associated withcondensins, cohesins, and other complexes involved in chromosome-related functions. Genome Res. 10, 1445–1452 (2000). doi: 10.1101/gr.147400; [PubMed: 11042144]

32. Lima CD, Wang LK, Shuman S, Structure and mechanismof yeast RNA triphosphatase: An essential component of the mRNA capping apparatus. Cell 99, 533–543 (1999). doi: 10.1016/S0092-8674(00)81541-X; [PubMed: 10589681]

33. Leung SS, Koslowsky DJ, Mapping contacts between gRNAand mRNA in trypanosome RNA editing. Nucleic Acids Res. 27, 778–787 (1999). doi: 10.1093/nar/27.3.778; [PubMed: 9889273]
34. Reifur L, Koslowsky DJ, Trypanosoma brucei ATPase subunit6 mRNA bound to gA6–14 forms a conserved three-helical structure. RNA 14, 2195–2211 (2008). doi: 10.1261/rna.1144508; [PubMed: 18772247]
35. Cooper S, Wadsworth ES, Schnaufer A, Savill NJ, Organization of minicircle cassettes and guide RNA genes in Trypanosoma brucei. RNA 28, 972–992 (2022). doi: 10.1261/rna.079022.121; [PubMed: 35414587]
36. Mattiacio JL, Read LK, Roles for TbDSS-1 in RNAsurveillance and decay of maturation by-products from the 12S rRNA locus. Nucleic Acids Res. 36, 319–329 (2008). doi: 10.1093/nar/gkm690; [PubMed: 18032430]
37. Zimmer SL, McEvoy SM, Li J, Qu J, Read LK, A novelmember of the RNase D exoribonuclease family functions in mitochondrial guide RNA metabolism in Trypanosoma brucei. J. Biol. Chem. 286, 10329–10340 (2011). doi: 10.1074/jbc.M110.152439; [PubMed: 21252235]
38. Sement FM et al. , Transcription initiation defines kinetoplast RNA boundaries. Proc. Natl. Acad. Sci. U.S.A. 115, E10323–E10332 (2018). doi: 10.1073/pnas.1808981115; [PubMed: 30333188]
39. Cech TR, RNA editing: World's smallest introns? Cell 64, 667–669 (1991). doi: 10.1016/0092-8674(91)90494-J; [PubMed: 1997201]
40. Aphasizhev R, Aphasizheva I, Simpson L, A tale of two TUTases. Proc. Natl. Acad. Sci. U.S.A. 100, 10617–10622 (2003). doi: 10.1073/pnas.1833120100; [PubMed: 12954983]
41. Foda BM, Downey KM, Fisk JC, Read LK, Multifunctional G-rich and RRM-containing domains of TbRGG2 perform separate yet essential functions in trypanosome RNA editing. Eukaryot. Cell 11, 1119–1131 (2012). doi: 10.1128/EC.00175-12; [PubMed: 22798390]
42. Van Nostrand EL et al. , Robust, Cost-Effective Profiling of RNA Binding Protein Targets with Single-end Enhanced Crosslinking and Immunoprecipitation (seCLIP). Methods Mol. Biol.1648, 177–200 (2017). doi: 10.1007/978-1-4939-7204-3_14; [PubMed: 28766298]
43. McAdams NM, Simpson RM, Chen R, Sun Y, Read LK,MRB7260 is essential for productive protein-RNA interactions within the RNA editing substrate binding complex during trypanosome RNA editing. RNA 24, 540–556 (2018). doi: 10.1261/rna.065169.117; [PubMed: 29330168]
44. McAdams NM et al. , MRB10130 is a RESC assembly factor that promotes kinetoplastid RNA editing initiation and progression. RNA 25, 1177–1191 (2019). doi: 10.1261/rna.071902.119; [PubMed: 31221726]
45. Igo RP Jr., Lawson SD, Stuart K, RNA sequence andbase pairing effects on insertion editing in Trypanosoma brucei. Mol. Cell. Biol. 22, 1567–1576 (2002). doi: 10.1128/MCB.22.5.1567-1576.2002; [PubMed: 11839822]
46. Lawson SD, Igo RP Jr., R. Salavati, K. D. Stuart, Thespecificity of nucleotide removal during RNA editing in Trypanosoma brucei. RNA 7, 1793–1802 (2001). doi: 10.1017/S135583820101055X; [PubMed: 11780635]
47. Igo RP Jr., Palazzo SS, Burgess ML, Panigrahi AK, Stuart K, Uridylate addition and RNA ligation contribute to the specificity of kinetoplastid insertion RNA editing. Mol. Cell. Biol.20, 8447–8457 (2000). doi: 10.1128/MCB.20.22.8447-8457.2000; [PubMed: 11046141]
48. Trotter JR, Ernst NL, Carnes J, Panicucci B, Stuart K,A deletion site editing endonuclease in Trypanosoma brucei. Mol. Cell 20, 403–412 (2005). doi: 10.1016/j.molcel.2005.09.016; [PubMed: 16285922]
49. Carnes J, Trotter JR, Ernst NL, Steinberg A, Stuart K, Anessential RNase III insertion editing endonuclease in Trypanosoma brucei. Proc. Natl. Acad. Sci. U.S.A. 102, 16614–16619 (2005). doi: 10.1073/pnas.0506133102; [PubMed: 16269544]
50. Lenarčič T. et al. , Mitoribosomal small subunit maturation involves formation of initiation-like complexes. Proc. Natl. Acad.Sci. U.S.A. 119, e2114710118 (2022). doi: 10.1073/pnas.2114710118;
51. Feagin JE, Shaw JM, Simpson L, Stuart K, Creation ofAUG initiation codons by addition of uridines within cytochrome b transcripts of kinetoplastids. Proc. Natl. Acad. Sci. U.S.A. 85, 539–543 (1988). doi: 10.1073/pnas.85.2.539; [PubMed: 2448777]

52. Kumar V. et al. , REH2C Helicase and GRBC Subcomplexes May Base Pair through mRNA and Small Guide RNA in Kinetoplastid Editosomes. J. Biol. Chem. 291, 5753–5764 (2016). doi: 10.1074/jbc.M115.708164; [PubMed: 26769962]

53. Hernandez A. et al. , REH2 RNA helicase in kinetoplastid mitochondria: Ribonucleoprotein complexes and essential motifs for unwinding and guide RNA (gRNA) binding. J. Biol. Chem. 285, 1220–1228 (2010). doi: 10.1074/jbc.M109.051862; [PubMed: 19850921]

54. Zhang L, bioliyezhang/RESC_paper, version v1.0.0, Zenodo (2023); doi: 10.5281/zenodo.7930544

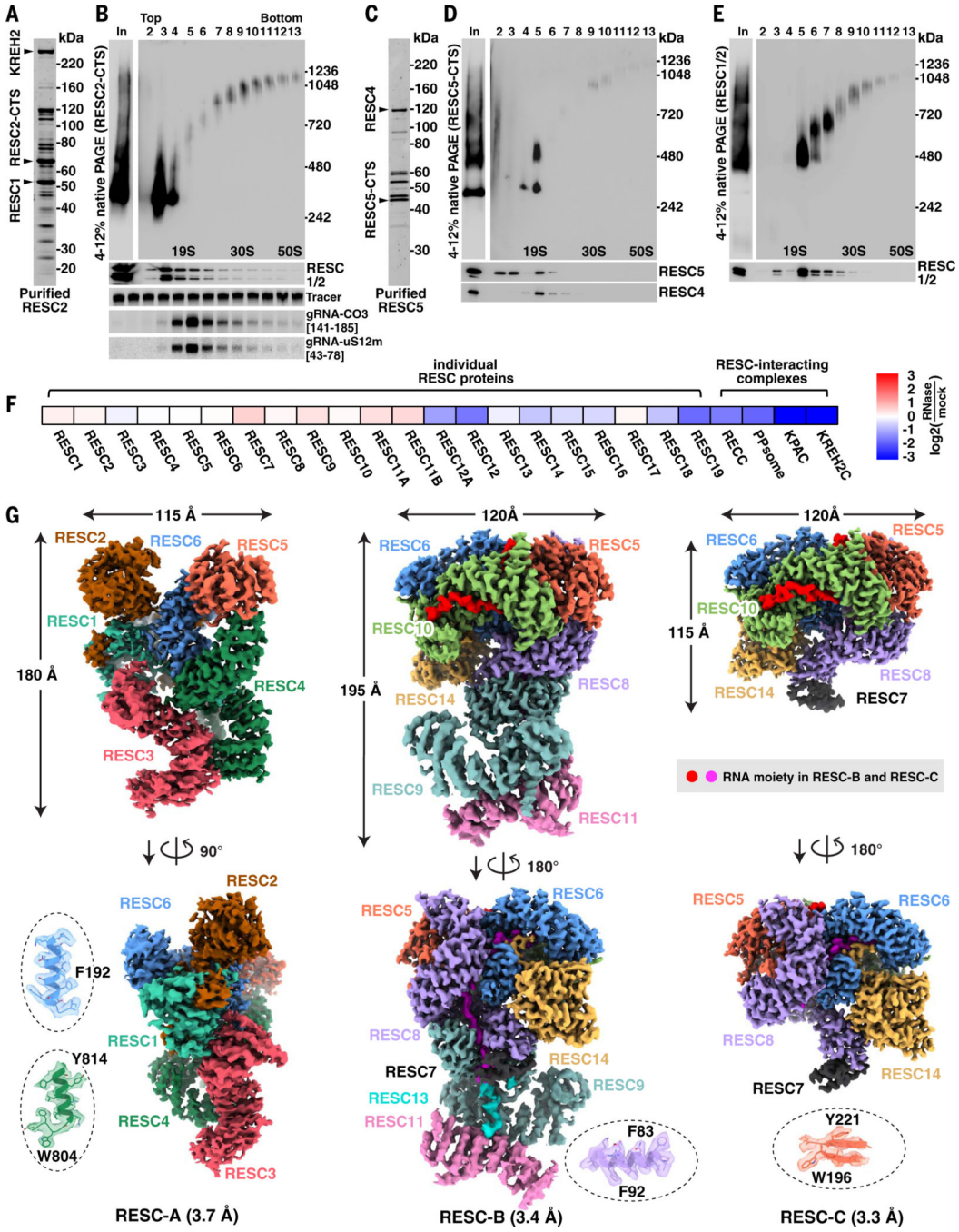

Fig. 1. Overall architecture of RESC-A, -B, and -C complexes from *T. brucei*.

(**A**) Tandem affinity–purified CTS-tagged RESC2 separated by means of SDS-PAGE and stained with fluorescent dye. Arrows indicate gRNA-binding proteins RESC1 and RESC2 and DEAH/RHA RNA helicase KREH2.(**B**) RESC2-CTS isolate separated by means of native PAGE (left) or glycerol gradient and then native PAGE (right), and visualized by immunoblot with a tag-specific antibody. Sedimentation rate values (S) of thyroglobulin, and small and large bacterial ribosomal subunits align with fractions probed for RESC1/2 (top; immunoblot with antibodies recognizing both proteins) and gRNAs CO3 (141 to

185) and uS12m (43 to 78]) (bottom; northern blot). Synthetic radiolabeled tracer shows uniformity of RNA isolation from gradient fractions (middle). (**C**) Tandem affinity–purified CTS-tagged RESC5 separated by means of SDS-PAGE and stained with fluorescent dye. (**D**) RESC5-CTS isolate separated by means of native PAGE (left), or by glycerol gradient and then native PAGE (right) and visualized with tag-specific antibody. RESC4 and RESC5 were detected in each fraction by immunoblot. (**E**) Membranes shown in (D) probed with antibodies against RESC1/2. (**F**) Relative abundances of RESC proteins and RNA-editing catalytic (RECC), mRNA stabilizing (PPsome), polyadenylation (KPAC), and KREH2 RNA helicase (KREH2C) complexes in RESC5 isolates from mock- and RNase-treated extracts. Heatmap represents log2-fold change values. RNase treatment of the extract prevented RESC5 co-isolation with RECC, PPsome, KPAC, and KREH2C; RESC12 and RESC12A paralogs also declined. Supporting mass spectrometry data are provided in table S2. (**G**) Distinct views of RESC-A (left), RESC-B (middle), and RESC-C (right) cryo-EM density maps. (Insets) Models overlayed on transparent cryo-EM density. Additional overlays are provided in fig. S9.

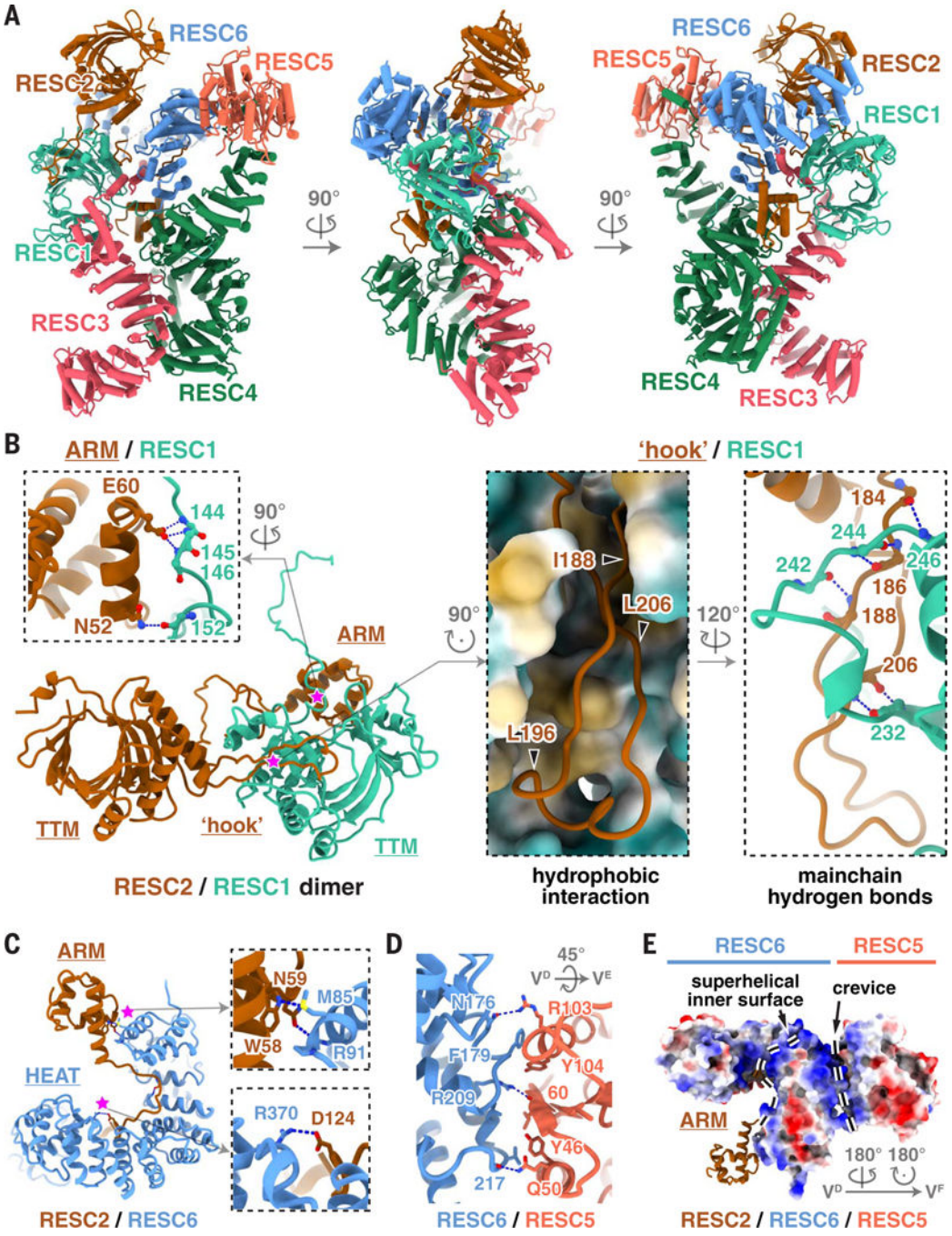

Fig. 2. Structure of RESC-A protein complex.

(**A**) Perpendicular views of the overall RESC-A assembly. (**B**) Magenta stars point to close-up views of interacting regions in the RESC1/2 heterodimer, detailing interactions between the ARM domains of RESC2 and RESC1 (top left) and between the RESC2 "hook" domain and RESC1 (right). Yellow patches color hydrophobic interactions with RESC2, presented as a strand, and RESC1, shown as a surface. (**C**) The C-terminal loop of the RESC2 ARM domain engages the inner surface of the RESC6 HEAT domain superhelix. Magenta stars point to expanded views of amino acid residues in the contacting regions. (**D**) Side-chain

interactions between RESC5 and RESC6. (**E**) Electrostatic surface potential of the RESC5/6 heterodimer.

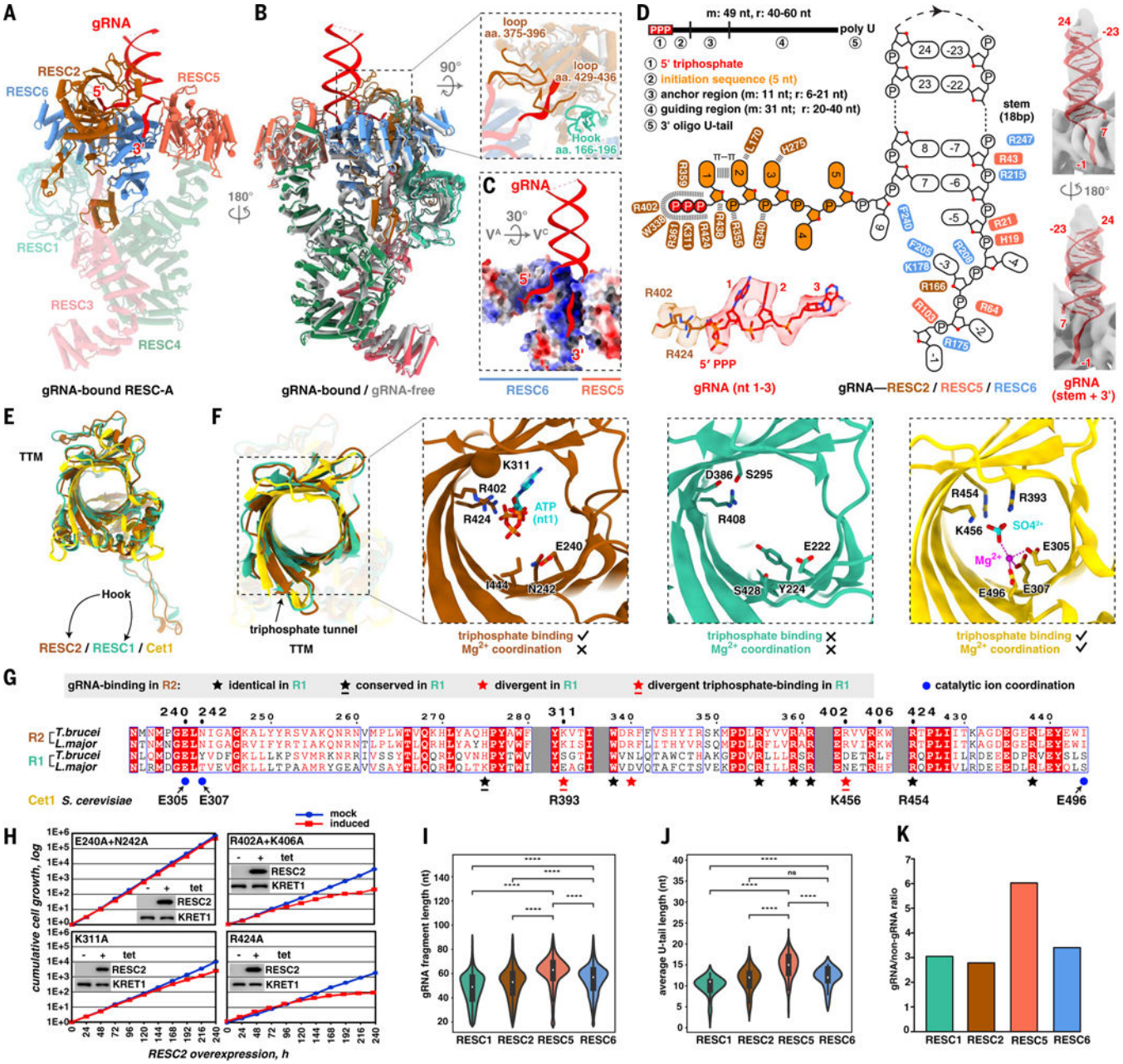

Fig. 3. Structure of RESC-A complex with gRNA.

(**A**) The gRNA binding RESC1/2 and RESC5/6 heterodimers and gRNA are highlighted in the overall RESC-A structure. (**B**) Disordered loops in RNA-depleted RESC-A become structured and visible with bound gRNA. (**C**) The 3′ terminus of gRNA occupies the positively charged crevice formed by RESC5 and RESC6. (**D**) Interactions between gRNA and gRNA-binding proteins. An atomic model was built for the first three nucleotides, with the triphosphate group visible on the first nucleotide. The rest of gRNA moiety was traced with the main chain. The model overlayed on transparent cryo-EM density map was shown for the first nucleotides of gRNA (bottom left) and the gRNA stem and the 3′ fragment (right). *m*, median length; *r*, range. (**E**) Superimposition of triphosphate tunnel

metalloenzyme (TTM) domains from RESC2 (brown), RESC1 (turquoise), and *S. cerevisiae* RNA triphosphatase Cet1 (yellow). (**F**) Focused views of RNA 5′ triphosphate-binding and catalytic metal ion–coordination sites in RESC2, RESC1, and Cet1. (**G**) Multiple sequence alignment of the TTM domains in RESC2 (R2) and RESC1 (R1). Red background depicts identical residues. Conserved residues are colored in red, and divergent residues are in black. gRNA-binding residues in RESC2 are labeled with stars; underlined red stars indicate RESC2 triphosphate–binding side chains that are divergent in RESC1. Cet1 residues structurally homologous to RESC2 positions are numbered; blue circles indicate catalytic metal-binding triad. (**H**) Growth kinetics of parasite cell lines that conditionally express mutated RESC2 proteins. (Insets) RESC2 expression in mock (–tet) cells and cells that were tetracycline-induced for 72 hours (+tet). KRET1, loading control. (**I**) Size distribution of gRNA fragments cross-linked to RESC1, RESC2, RESC5, and RESC6. ****$q < 0.0001$, Welch's t test followed by Benjamini–Hochberg (BH) false discovery rate (FDR) correction. (J) Distribution of average U-tail length in gRNAs fragments cross-linked to RESC1, RESC2, RESC5, and RESC6. ****$q < 0.0001$; ns, not significant. Mann-Whitney U test, followed by BH FDR correction. (**K**) Ratios of gRNAs versus minicircle-encoded gRNA-like molecules cross-linked to RESC-A subunits. Single-letter abbreviations for the amino acid residues are as follows: A, Ala; E, Glu; K, Lys; R, Arg; N, Asn.

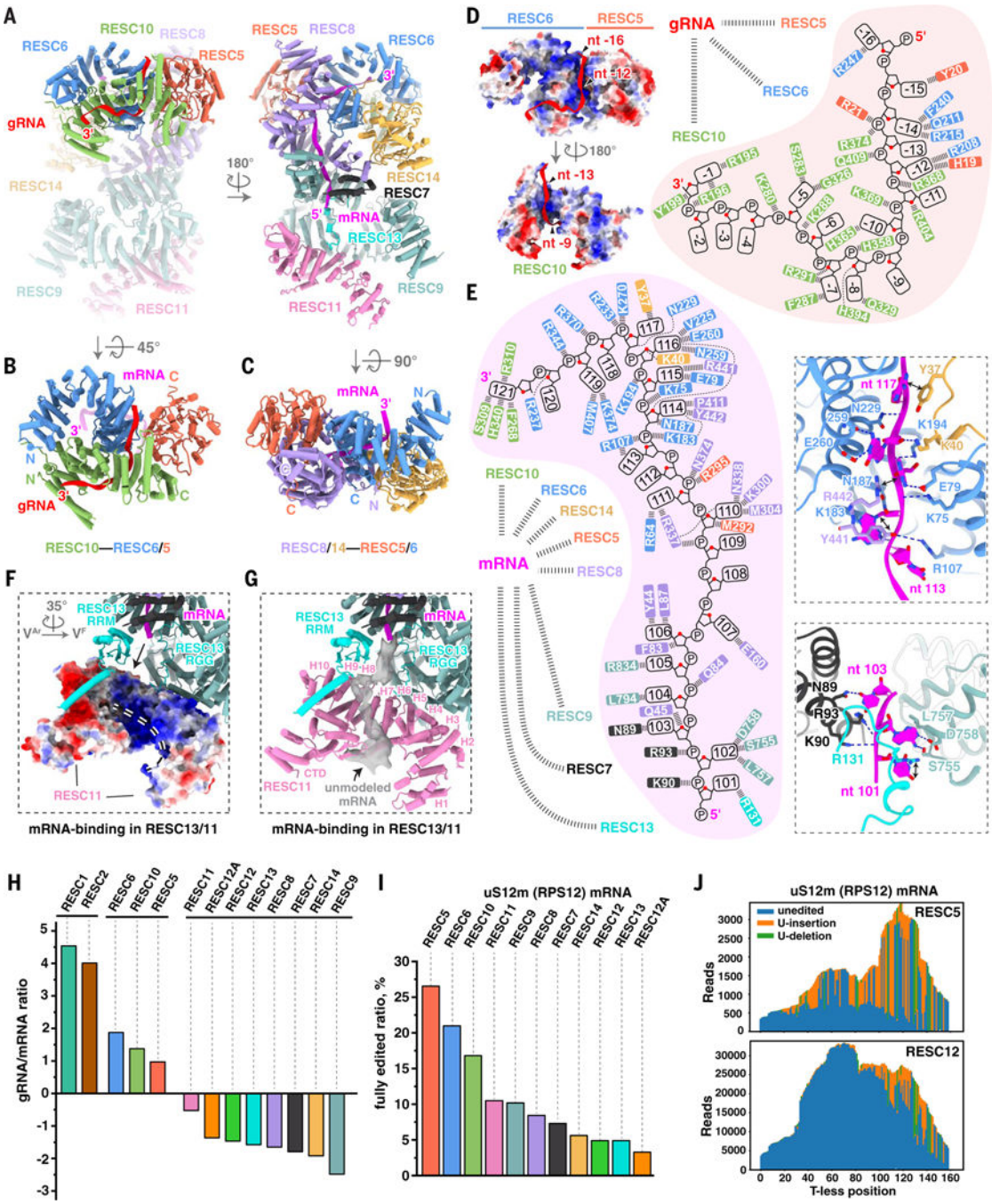

Fig. 4. gRNA and mRNA trajectories in RESC-B complex.

(**A**) Overall RESC-B structure. (Left) gRNA-interacting proteins RESC5, RESC6, and RESC10 and gRNA moiety. (Right) mRNA-binding proteins RESC5, RESC6, RESC7, RESC8, RESC9, and RESC11 and the mRNA reconstitution. (**B**) Binding of gRNA and mRNA fragments by RESC5, RESC6, and RESC10. (**C**) Binding of the mRNA's 3′ region by RESC5, RESC6, RESC8, and RESC14. (**D**) Electrostatic interactions between gRNA and RESC5, RESC6, and RESC10. Blue surfaces show positively charged grooves. (**E**) Interactions between mRNA and RESC-B residues. Close-up views show the detailed

interaction of RESC7, RESC9, and RESC13 with mRNA positions 101 to 103, and those of RESC6, RESC8, and RESC14 with positions 113 to 117. (**F** and **G**) Potential architecture of mRNA 5′-end binding site shaped by RESC11 and RESC13. (F) RESC11 is shown as electrostatic surface potential, whereas RESC13 is shown as ribbon. (G) RESC11/RESC13 are shown as ribbon, whereas unmodeled mRNA is shown as transparent gray density. Double-dashed line indicates positively charged surface area. (**H**) In vivo gRNA-mRNA binding preferences of RESC proteins. Reads were mapped to annotated gRNAs (35) and to 12 edited mRNA genes in all editing states. Read-count ratios are log2-transformed and centered by the average of all RESC proteins. (**I**) Prevalence of fully edited uS12m (RPS12) mRNA sequences detected with in vivo UV cross-linking analysis of RESC-B proteins. The ratio of fully edited to combined pre-, partially, and fully edited mRNA fragments is plotted for each RESC-B subunit. (**J**) Positional mapping of RESC5 and RESC12 in-vivo binding sites in uS12m (RPS12) mRNA. The x axis represents 5′-to-3′ mRNA coordinates after removing encoded Us and those inserted by editing (T-less). The y axis shows the total read depth for pre-edited (blue), U-insertions (orange), and U deletions (green) per nucleotide.

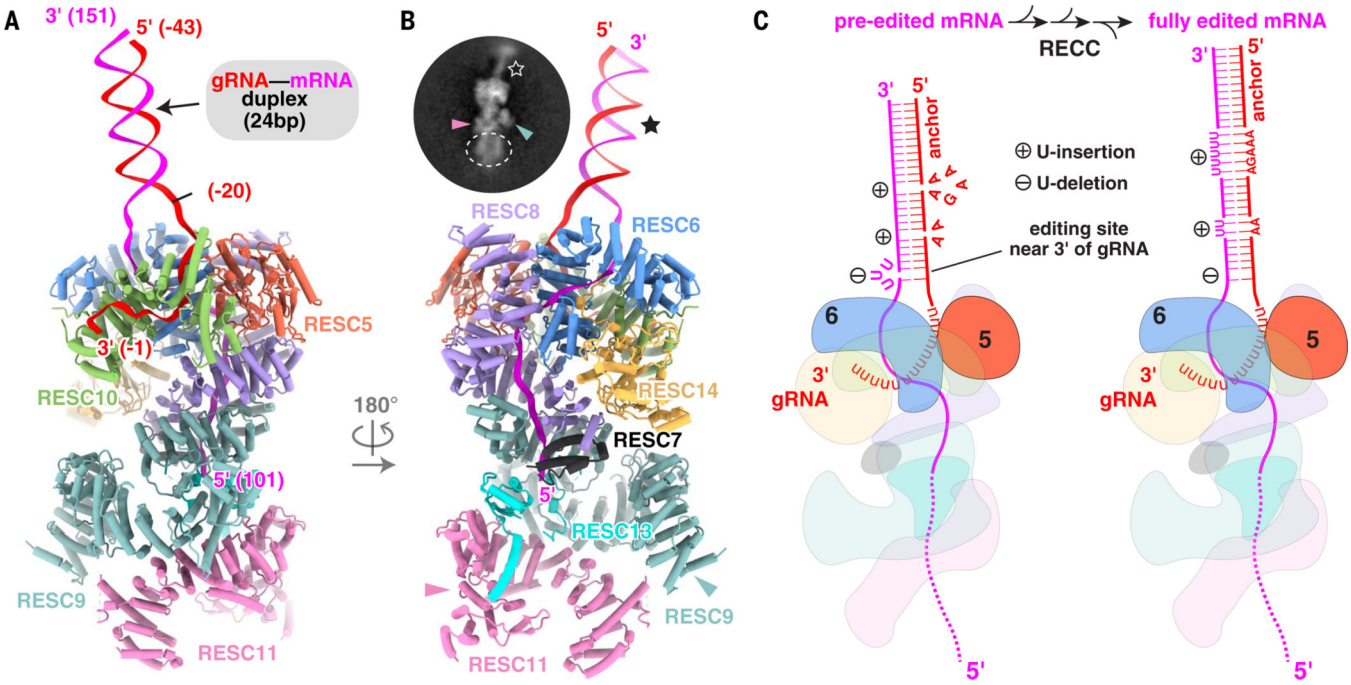

Fig. 5. Overall architecture of gRNA-mRNA hybrid exiting RESC-B.

(**A** and **B**) Flipped views of the 24-bp duplex between gRNA and edited mRNA protruding out of RESC5, RESC6, RESC8, and RESC10. Three-dimensional (3D) projection of the cryo-EM map in (B) shows the gRNA-mRNA duplex (black star) and putative RESC12/12A (dashed circle). This 2D class average shares the same view as the RESC-B structure shown underneath. (**C**) A model of RNA-editing substrate. Mismatches in the duplex between gRNA and pre-edited mRNA delineate U-insertion (+) and U-deletion (–) editing sites (left). Completion of editing events extends the double-stranded region initially formed by the anchor through the guiding gRNA parts until full complementarity is achieved (right).

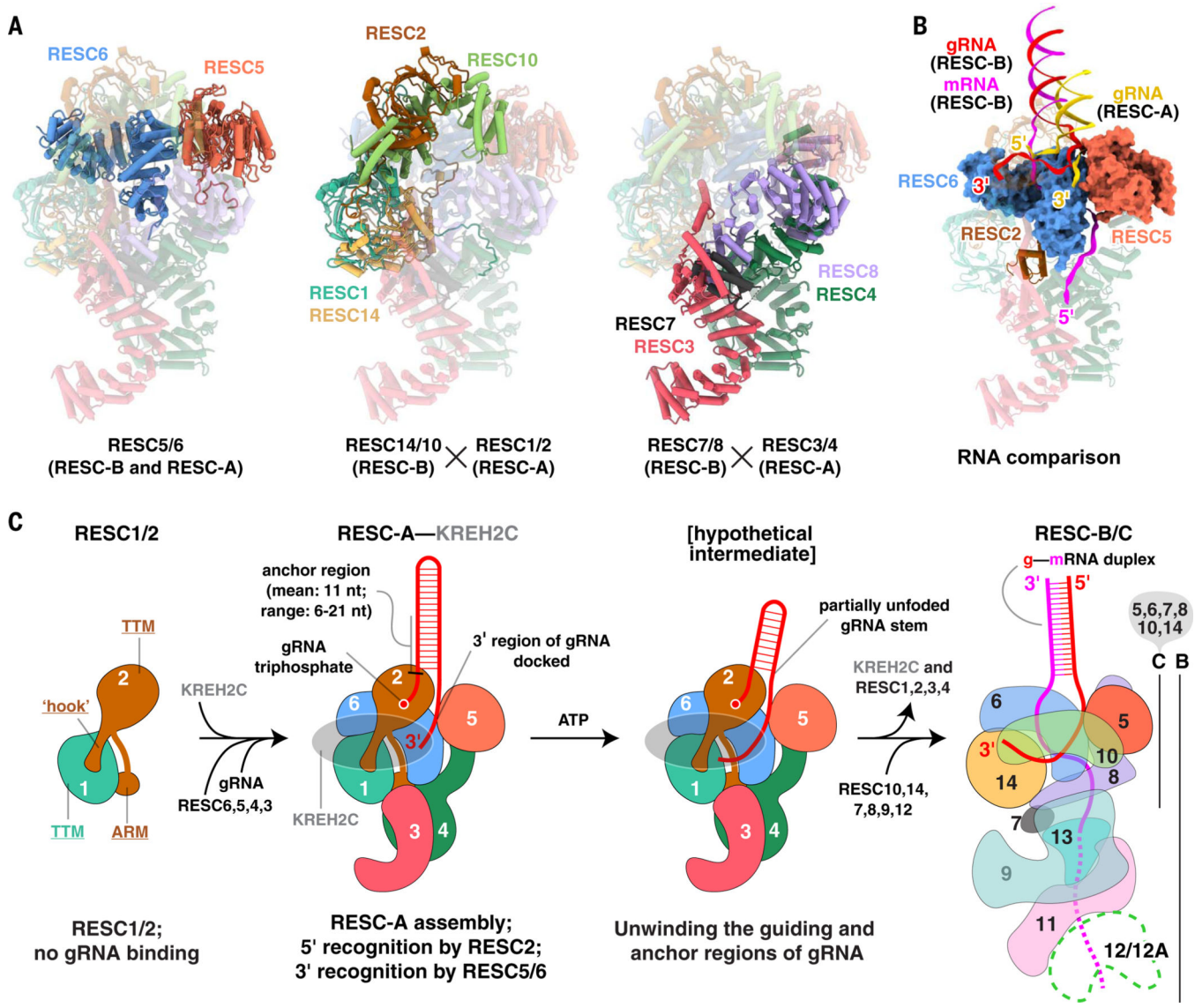

Fig. 6. Model of transition from RESC-A to RESC-B.

(**A**) Potential clashes resolved by remodeling of RESC-A to RESC-B. RESC5 and RESC6 are well aligned in both complexes (left); RESC14/10 in RESC-B replace RESC1/2 in RESC-A (middle), and RESC7/8 in RESC-B replace RESC3/4 in RESC-A (right). RESC9 and RESC12 positioned in RESC-B midsection do not collide with RESC-A proteins. (**B**) Comparison of RESC-A and RESC-B highlights the preservation of RESC5/6 (surface) and repositioning of gRNA's single-stranded 3′ end (ribbon). RESC-B proteins are not shown for better visualization. (**C**) Proposed model of gRNA-stabilizing RESC-A assembly and KREH2C-induced remodeling into the editing-competent RESC-B.